ISSN (Print) 1226-1750
ISSN (Online) 2233-6656
Journal of Magnetics 27(3), 293-297 (2022) https://doi.org/10.4283/JMAG.2022.27.3.293

Improving the Soft Magnetic Properties of Fe-Co-B-Zr-Nb Alloy by Tuning the Fe/Co Ratio

Jihye Park and Haein Choi-Yim*

Department of Applied Physics, Sookmyung Women's University, Seoul 04310, Republic of Korea

(Received 2 September 2022, Received in final form 15 September 2022, Accepted 15 September 2022)

Amorphous $(Fe_xCo_{1-x})_{85}B_5Zr_yNb_{10-y}$ (x = 0.6, 0.7, 0.8, or 0.9 and y = 7 or 8 at.%) ribbons were fabricated by the melt-spinning technique, and their thermal and magnetic properties were investigated. The results showed that all alloys had a fully amorphous structure, and the substitution of Zr for Nb resulted in high thermal stability and high saturation flux density (B_s) with fairly low coercivity (H_c < 21 A/m). Moreover, by varying the Fe/Co ratio, the optimum ratio with the highest B_s and low H_c was determined. As the Fe/Co ratio changed from 6:4 to 9:1, H_c decreased from approximately 20 to 9 A/m, and B_s also decreased gradually. A saturation flux density of 1.33 T was achieved with a coercivity of 9 A/m after optimization.

Keywords : Fe-based, amorphous, soft magnetic material, ribbon

1. Introduction

Soft magnetic materials are essential for the efficient operation of next-generation power electronics and electrical machinery such as motors, generators, and transformers [1, 2]. Further, the demand for high efficiency, automation, and miniaturization of devices is increasing the use of soft magnetic materials with low core loss, high magnetic flux density (B_s), and high permeability (μ_e) [3-5]. Over the past few decades, various types of soft magnetic materials have been used, including electrical steel, Fe, Ni-Zn/Mn-Zn ferrite, Fe-Ni, Fe-Si, Fe-Si-Al, nanocrystalline alloys, and metallic glassy metals [3, 6, 7].

Amorphous alloys have attracted much attention owing to their unique atomic arrangement that differs from those of typical crystalline materials [8, 9]. This unique arrangement affords a combination of mechanical characteristics, including high breaking strength, high elasticity, high wear resistance, high corrosion resistance, and excellent soft magnetic properties [10-12]. Furthermore, Fe-based amorphous/nanocrystalline alloys have approximately 100 times higher permeability, 100 times lower coercive force, and five times lower iron loss compared to existing crystalline soft magnetic materials such as Fe-Si and Fe-Si-Al alloys [13, 14]. Therefore, they are emerging as optimal materials for producing high-performance and high-efficiency magnetic parts. Amorphous and nanocrystalline materials are constantly being improved through increases in B_s and the introduction of new alloys that are more amenable to fabricating large-scale parts [1, 15-18]. Well-known alloys include FINEMET (Yoshizawa *et al.*, 1988), NANOPERM (Suzuki *et al.*, 1988), HITPERM (Willard *et al.*, 1998), and NANOMET (Makino *et al.*, 2011). Among these, the Fe-Co-Zr-B-Cu alloy HITPERM exhibits high B_s and better soft magnetic properties than those of other families of materials at high temperatures [2, 19-21]. Škorvánek *et al.* experimentally demonstrated that Cu-free HITPERM exhibits a remarkably lower H_c than that of the original HITPERM [22]. Therefore, copper is not necessary to form the ultrafine structure of HITPERM. Additionally, an appropriate composition of Zr and Nb can be used to control the thermal stability while maintaining the B_s, μ_e, and mean grain size [23, 24].

The present study investigates the effects of Zr substitution for Nb with varying Fe/Co ratios in $(Fe_xCo_{1-x})_{85}B_5Zr_yNb_{10-y}$ (x = 0.6, 0.7, 0.8, or 0.9 and y = 7 or 8 at.%) alloys on the magnetic and thermal properties.

2. Experimental Procedure

Alloys with a nominal composition of $(Fe_xCo_{1-x})_{85}B_5Zr_yNb_{10-y}$ (x = 0.6, 0.7, 0.8, or 0.9 and y = 7 or 8 at.%)

*Corresponding author: Tel: +82-2-710-9239
e-mail: haein@sookmyung.ac.kr

were studied. The ingots were prepared by arc melting under Ar atmosphere with high-purity Fe (99.95 %), Co (99.95 %), Zr (99.5 %), Nb (99.95 %), and B (99.5 %). All ingots were remelted at least four times to ensure that the alloys were homogeneously mixed. The melt-spinning technique was used to fabricate rapidly solidified amorphous ribbons having a width and thickness of 2 mm and 20-30 μm, respectively, with a roller speed of 56.3 m/s. Differential scanning calorimeter (DSC) was used to evaluate thermal stability at a heating rate of 0.34 K/s under Ar gas flow. The structural property of the amorphous ribbons was characterized by X-ray diffraction (XRD) with Cu-Kα radiation. The magnetic measurement was performed using a vibrating sample magnetometer (VSM) and DC B-H loop tracer. The saturation magnetization (M_s) was measured using a VSM under an in-plane applied field ranging from −800 to 800 kA/m, and H_c was measured using a DC B-H loop tracer.

3. Results and Discussion

Figure 1 shows the X-ray Diffraction patterns of the melt-spun $(Fe_xCo_{1-x})_{85}B_5Zr_yNb_{10-y}$ (x = 0.6, 0.7, 0.8, or 0.9 and y = 7 or 8 at.%) alloys with varying Fe/Co ratios. Broad diffraction peaks were observed at diffraction angles of 2θ ≈ 44°. No peaks correspond to any crystalline phase in all alloys. Fe/Co ratios of 6:4 to 9:1 had no effect on the amorphization procedure, and the alloy system retained an amorphous structure.

Figure 2 shows the DSC curves of the $(Fe_xCo_{1-x})_{85}B_5$-Zr_yNb_{10-y} (x = 0.6, 0.7, 0.8, or 0.9 and y = 7 or 8 at.%) ribbons. All alloys show distinct exothermic peaks, indicating the precipitation of the α-Fe phase [25, 26]. Figure 2 shows the crystallization onset temperatures (T_x) of the alloys. With increasing Fe content, the T_x of $(Fe_xCo_{1-x})_{85}B_5Zr_7Nb_3$ (alloys with y = 3 at.% and x = 0.6, 0.7, 0.8, or 0.9, hereinafter denoted as Zr7 alloys) and

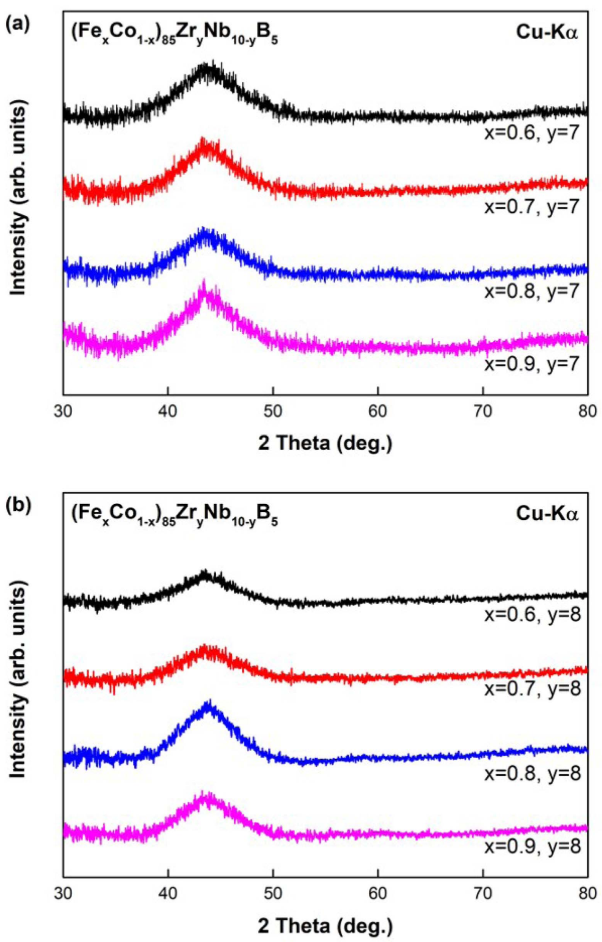

Fig. 1. XRD patterns of (a) $(Fe_xCo_{1-x})_{85}B_5Zr_8Nb_2$ (x = 0.6, 0.7, 0.8, or 0.9) and (b) $(Fe_xCo_{1-x})_{85}B_5Zr_7Nb_3$ (x = 0.6, 0.7, 0.8, or 0.9) as-spun ribbons.

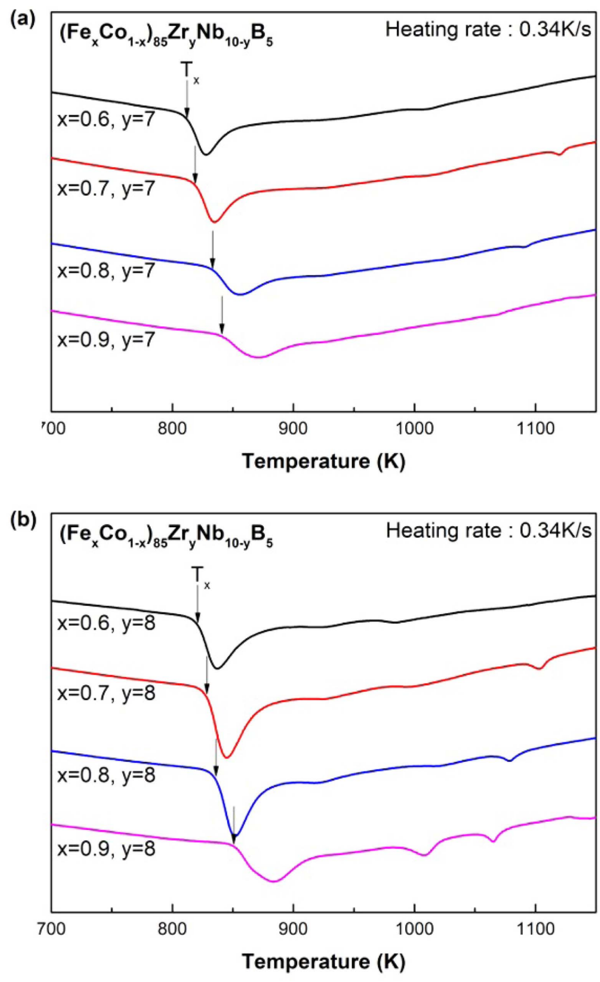

Fig. 2. DSC curves of (a) $(Fe_xCo_{1-x})_{85}B_5Zr_8Nb_2$ (x = 0.6, 0.7, 0.8, or 0.9) and (b) $(Fe_xCo_{1-x})_{85}B_5Zr_7Nb_3$ (x = 0.6, 0.7, 0.8, or 0.9) as-spun ribbons.

Table 1. Thermal and magnetic properties of as-spun $(Fe_xCo_{1-x})_{85}B_5Zr_{10-y}Nb_y$ (x = 0.6, 0.7, 0.8, or 0.9 and y = 2 or 3 at.%) ribbons.

Alloys						Thermal Properties	Magnetic Properties		
Fe/Co Ratio	Alloy Composition					T_x (K)	H_c (A/m)	M_s (emu/g)	B_s (T)
6:4	Fe_{51}	Co_{34}	Zr_8	Nb_2	B_5	820	21	139.80	1.35
7:3	$Fe_{59.5}$	$Co_{25.5}$	Zr_8	Nb_2	B_5	828	17	137.05	1.34
8:2	Fe_{68}	Co_{17}	Zr_8	Nb_2	B_5	836	15	128.37	1.23
9:1	$Fe_{76.5}$	$Co_{8.5}$	Zr_8	Nb_2	B_5	850	9	100.15	1.05
6:4	Fe_{51}	Co_{34}	Zr_7	Nb_3	B_5	812	19	135.78	1.33
7:3	$Fe_{59.5}$	$Co_{25.5}$	Zr_7	Nb_3	B_5	819	9	135.70	1.32
8:2	Fe_{68}	Co_{17}	Zr_7	Nb_3	B_5	833	9	128.57	1.24
9:1	$Fe_{76.5}$	$Co_{8.5}$	Zr_7	Nb_3	B_5	841	7	110.86	0.95

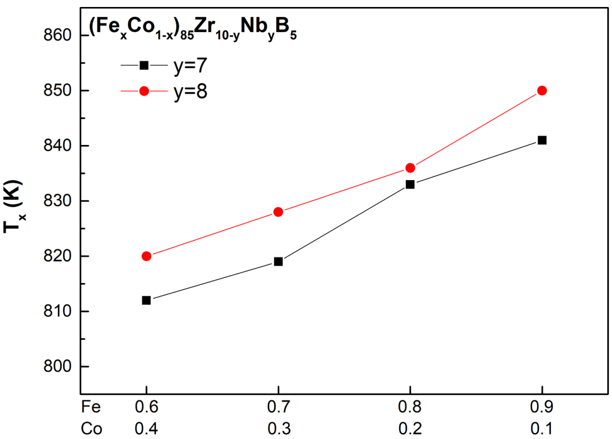

Fig. 3. Variation of the crystallization temperature (T_x) of the as-spun ribbons of $(Fe_xCo_{1-x})_{85}B_5Zr_{1-y}Nb_y$ (x = 0.6, 0.7, 0.8, or 0.9 and y = 2 or 3 at.%).

$(Fe_xCo_{1-x})_{85}B_5Zr_8Nb_2$ (alloys with y = 2 at.% and x = 0.6, 0.7, 0.8, or 0.9, hereinafter denoted as Zr8 alloys) ribbons increased from 812 to 841 K and from 820 to 850 K, respectively. Because T_x serves as a reference for the upper temperature limit for improving the magnetic properties, increasing the T_x value is highly desirable. In addition, a rapidly increasing T_x value is more likely to expand the supercooled region, which can increase the thermal stability. Based on DSC data, the crystallization temperature was plotted as a function of the Fe/Co ratios in Fig. 3. The graph shows that all T_x values for Zr8 alloys were higher than those for Zr7 alloys for a given Fe/Co ratio. Combined with previous research [27] that reports data for $(Fe_xCo_{1-x})_{85}B_5Zr_9Nb_1$ (x = 0.6, 0.7, 0.8, or 0.9) alloys, increasing the Zr content in the Fe-Co-B-Zr-

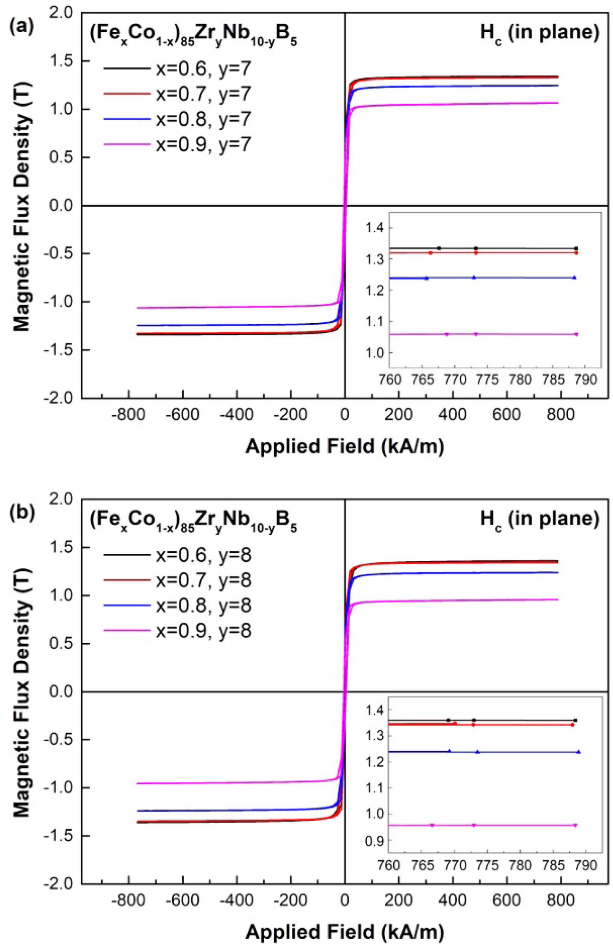

Fig. 4. B-H curves of (a) $(Fe_xCo_{1-x})_{85}B_5Zr_8Nb_2$ (x = 0.6, 0.7, 0.8, or 0.9) and (b) $(Fe_xCo_{1-x})_{85}B_5Zr_7Nb_3$ (x = 0.6, 0.7, 0.8, or 0.9) ribbons in as-quenched state.

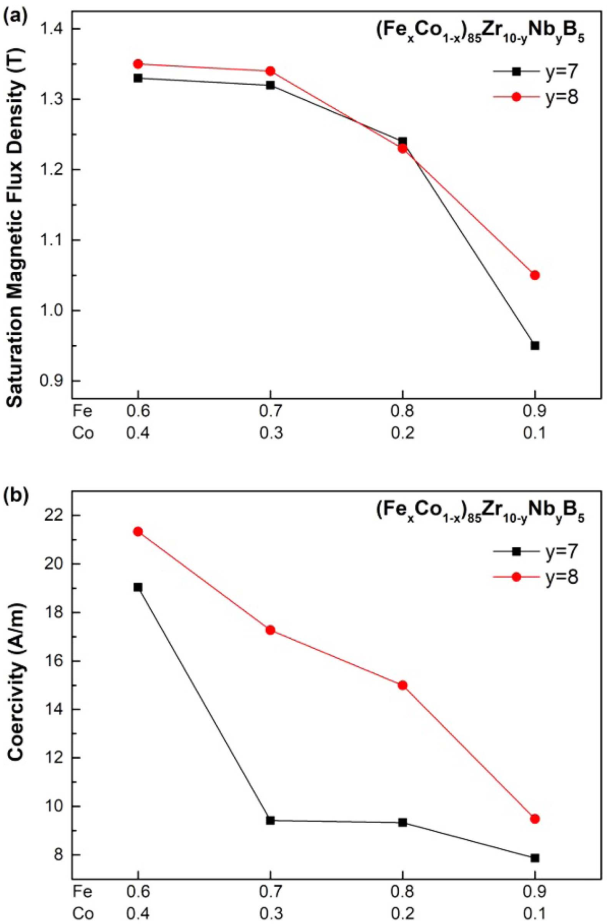

Fig. 5. Dependence of B_s and H_c on Fe/Co ratio of $(Fe_xCo_{1-x})_{85}$-$B_5Zr_{10-y}Nb_y$ (x = 0.6, 0.7, 0.8, or 0.9 and y = 2 or 3 at.%) melt-spun ribbons.

Nb system can increase the crystallization temperature.

Figure 4 shows the B-H hysteresis loops of the $(Fe_xCo_{1-x})_{85}B_5Zr_{10-y}Nb_y$ (x = 0.6, 0.7, 0.8, or 0.9 and y = 7 or 8 at.%) melt-spun ribbons. All curves exhibit the typical squared loop of soft magnetic materials. The saturated parts of the graphs are enlarged in the upper left corner to compare B_s values with the Fe/Co ratio. Figure 5 shows the B_s and H_c values of $(Fe_xCo_{1-x})_{85}B_5Zr_{10-y}Nb_y$ (x = 0.6, 0.7, 0.8, or 0.9 and y = 7 or 8 at.%) ribbons as functions of the Fe/Co ratio. Overall, Zr8 alloys showed higher B_s values compared with those of Zr7 alloys; however, in the case of H_c, Zr7 alloys have lower values for a fixed Fe/Co ratio. B_s shows an increasing trend as the Fe:Co ratio changes from 9:1 to 6:4. Specifically, it changes from 0.95 to 1.33 T for Zr7 alloys and from 1.05 to 1.35 T for Zr8 alloys, indicating that the highest B_s is achieved for an Fe/Co ratio of 6:4 for both Zr7 and Zr8 alloys. Furthermore, H_c shows a downward trend with increasing Fe content (Fig. 5); it decreases from 19 to 7 A/m (Zr7 alloys) and from 21 to 9 A/m (Zr8 alloys). In particular, for Zr7 alloys, when the Fe/Co ratio is changed from 6:4 to 7:3, B_s remains almost unchanged, whereas H_c decreases greatly; these alloys show the best soft magnetic properties.

4. Conclusion

We investigated changes in the amorphous forming ability and soft magnetic properties of Zr substituted for Nb in Fe-Co-B-Zr-Nb amorphous ribbons. Further, we varied the Fe/Co ratios to optimize the thermal and magnetic properties, and we drew the following conclusions.

The effects of substituting Zr for Nb on the T_x, B_s, and H_c values were observed. For all Fe/Co ratios, T_x and B_s increased with slightly increased H_c. Therefore, $(Fe_xCo_{1-x})_{85}$-$B_5Zr_7Nb_3$ alloys have better thermal and magnetic characteristics than those of $(Fe_xCo_{1-x})_{85}B_5Zr_8Nb_2$ alloys.

As the Fe/Co ratio changes from 6:4 to 9:1, T_x increases by 30 K, indicating that the Fe/Co ratio affects the thermal properties of the alloys, and that the thermal stability improves as the Fe content increases.

B_s and H_c both decrease as the Fe/Co ratio is varied from 4:6 to 9:1. The highest B_s value of 1.35 T is achieved when the Fe/Co ratio is 6:4; however, when the Fe/Co ratio reaches 7:3, B_s decreases slightly and H_c increases significantly, resulting in the optimum soft magnetic properties. For further improvement, heat treatment can be performed under appropriate conditions to reduce H_c and increase B_s.

References

[1] J. M. Silveyra, E. Ferrara, D. L. Huber, and T. C. Monson, Science **362**, 6413 (2018).
[2] R. S. Kumar and J. S. Rajan, 5NANO 1 (2022).
[3] H. J. Kim, J. Korean Magn. Soc. **21**, 77 (2011).
[4] B. S. Ram, A. K. Paul, and S. V. Kulkarni, J. Magn. Magn. Mater. **537**, 168210 (2021).
[5] W. D. Callister and D. G. Rethwisch, Materials Science and Engineering: An Introduction, John Wiley & Sons: New York, 5 (2011) pp 801-821.
[6] T. Abraham, JOM **47**, 16 (1995).
[7] R. S. Sundar and S. C. Deevi, Int. Mater. Rev. **50**, 157 (2005).
[8] M. E. McHenry, M. A. Willard, and D. E. Laughlin, Prog. Mater. Sci. **44**, 291 (1999).
[9] I. V. Zolotukhin and Y. E. Kalinin, Sov. Phys. Usp. **33**, 720 (1990).
[10] K. H. Chang, I. J. Shon, and C. S. Choi, Korean J. Kor. Inst. Met & Mater. **26**, 966 (1988).

[11] A. Inoue and A. Takeuchi, Mater. Sci. Eng. A **16**, 375 (2004).
[12] N. Yodoshi, R. Yamada, A. Kawasaki, and A. Makino, J. Alloys Compd. **612**, 243 (2014).
[13] V. S. Tsepelev and Y. N. Starodubtsev, Nanomaterials **11**, 108 (2021).
[14] S. Nakajima, Low-Loss Soft Magnetic Materials. In: Magnetic Material for Motor Drive Systems, Engineering Materials. Springer: Singapore (2019) pp 279-307.
[15] L. Guo, S. Geng, Z. Yan, Q. Chen, S. Lan, and W. Wang, Vacuum **199**, 110983 (2022).
[16] T. Liu, F. Li, A. Wang, L. Xie, Q. He, J. Luan, A. He, X. Wang, C. Liu, and Y. Yang, J. Alloy. Compd. **776**, 606 (2019).
[17] J. Tang, L. Zhou, D. Tan, and Y. Du, J. Alloy. Compd. **394**, 215 (2005).
[18] Y. Z. Chen, A. Herz, Y. J. Li, C. Borchers, P. Choi, D. Raabe, and R. Kirchheim, Acta Mater. **61**, 3172 (2013).
[19] M. A. Willard, M. Q. Huang, D. E. Laughlin, and M. E. McHenry, J. Appl. Phys. **85**, 4421 (1999).
[20] B. Kunca, J. Marcin, R. Parsons, P. Švec, P. Švecsr, K. Suzuki, and I. Škorvánek, J. Alloy. Compd. **911**, 165033 (2022).
[21] I. Škorvánek, J. Marcin, T. Krenický, J. Kováč, P. Švec, and D. Janičkovič, J. Magn. Magn. Mater. **304**, 203 (2006).
[22] I. Škorvánek, P. Švec, J. Marcin, J. Kováč, T. Krenický, and M. Deanko, Phys. Status Solidi A-Appl. Res. **196**, 217 (2003).
[23] A. Makino, T. Bitoh, A. Kojima, A. Inoue, and T. Masumoto, J. Magn. Magn. Mater. **215**, 288 (2000).
[24] A. Makino, T. Hatanai, Y. Naitoh, T. Bitoh, A. Inoue, and T. Masumoto, IEEE Trans. Magn. **33**, 3798 (1997).
[25] W. Q. Yu and L. P. Lu, IOP Conf. Ser.: Mater. Sci. Eng. **668**, 012003 (2019).
[26] B. Yao, Y. Zhang, L. Si, H. Tan, and Y. Li, J. Phys.-Condes. Matter. **16**, 6325 (2004).
[27] H. Son, G. Yoo, Q. Mustaghfiroh, D. H. Kim, and H. Choi-Yim, Metals. **12**, 12 (2021).